Journal of Solid State Chemistry **166,** 73–80 (2002)
doi:10.1006/jssc.2002.9562, available online at http://www.idealibrary.com on IDEAL®

An Electron Diffraction and Crystal Chemical Investigation of Oxygen/Fluorine Ordering in Niobium Oxyfluoride, NbO_2F

Frank J. Brink,[1,2] Ray L. Withers, and Lasse Norén

Research School of Chemistry, Australian National University, Canberra, ACT 0200, Australia

Received November 20, 2001; in revised form February 19, 2002; accepted February 22, 2002

A careful electron diffraction study of the ReO_3-type oxyfluoride NbO_2F has revealed the presence of characteristic transverse polarized planes of diffuse intensity running through the $G \pm \langle hk\frac{1}{3}\rangle^*$ regions of reciprocal space as well as continuous rods of diffuse intensity running through the $G \pm \langle \frac{11}{22}\xi\rangle^*$ regions of reciprocal space. The continuous planes of diffuse intensity in reciprocal space (perpendicular to each of the major crystal directions a, b and c) imply the existence of one-dimensional, oxygen/fluorine-ordered columns of atoms along $\langle 001\rangle$ in real space but with no lateral correlation in the ordering from such $\langle 001\rangle$ column to the next. The continuous lines of diffuse intensity along the $\langle \frac{11}{22}\xi\rangle^*$ directions of reciprocal space are ascribed to Rigid Unit Mode (RUM) rotations of the constituent MX_6 octahedral framework. A combination of bond-valence arguments and simple structure factor calculations are used to support this argument. © 2002 Elsevier Science (USA)

INTRODUCTION

NbO_2F is one member of a relatively small group of $MO_{3-x}F_x$ (M = Nb, Ta, Ti, Mo, W) oxyfluoride phases (1, 2) which are reported to have the simple cubic ReO_3 structure type (see Fig. 1). They have been of interest in recent years as host compounds for Li-insertion (3, 4) but also because of a pressure-induced structural phase transformation arising from a condensed Rigid Unit Mode (RUM) distortion of the simple cubic parent structure type (5, 6). The average structure (space group $Pm3m$) consists of corner-sharing MX_6 (X = O, F) octahedra (see Fig. 1) as in an undistorted ABO_3 perovskite structure with the A sites being empty.

To date these, and most other, oxyfluoride phases have been reported to exhibit only a statistical distribution of O and F onto the available anion sites (7, 8). This apparent random anion site disorder is generally attributed to oxygen and fluorine having similar size or ionic radii thus leading to no real preference in the site occupancies of any particular anion site. Bond-length/bond-strength calculations (9, 10), however, which take into account differences in electronegativity and charge of the anions, generally suggest that there should be a strong driving force for ordering.

Experimental evidence for oxygen/fluorine ordering is generally complicated by the difficulty of directly distinguishing oxygen from fluorine using common diffraction techniques such as X-ray, neutron or electron diffraction (11, 12). Where O/F ordering is complete and no disorder occurs, bond valence calculations can usually be used to distinguish the O-occupied sites from the F-occupied sites (8, 12). Where true long-range O/F ordering does not exist, however, it is necessary to look for more subtle diffraction features such as structured diffuse scattering, typically a consequence of the correlated displacive relaxation of the cations induced by local O/F ordering (13). When available, spectroscopic techniques such as NMR or Mössbauer (11, 13–15), which provide information regarding local coordination environments, can provide critical additional information essential in the formulation of a specific ordering model (see, for example, Ref. 13). In this paper, electron diffraction is used to search for evidence of O/F ordering in NbO_2F.

SYNTHESIS AND DATA COLLECTION

The NbO_2F used in this study was prepared (following the procedure of Frevel and Rinn (1)) by dissolving Nb powder in aqueous HF (48%), followed by evaporation of the excess liquid until dry. The resulting white powder was then dried further at 200°C for 48 h (1). Guinier XRD data confirmed that the end product was phase pure NbO_2F (a = 3.902(1) Å). Samples suitable for transmission electron microscopy (TEM) work were prepared by the dispersion of finely ground material onto a holey carbon film. Electron diffraction patterns (EDPs) were obtained using a Philips EM 430 TEM. A combination of Lucis® software (Image

[1]To whom correspondence should be addressed. E-mail brink@rsbs.anu.edu.au.

[2]Also at Electron Microscope Unit, Research School of Biological Sciences, Australian National University, Canberra ACT 0200, Australia.

0022-4596/02 $35.00

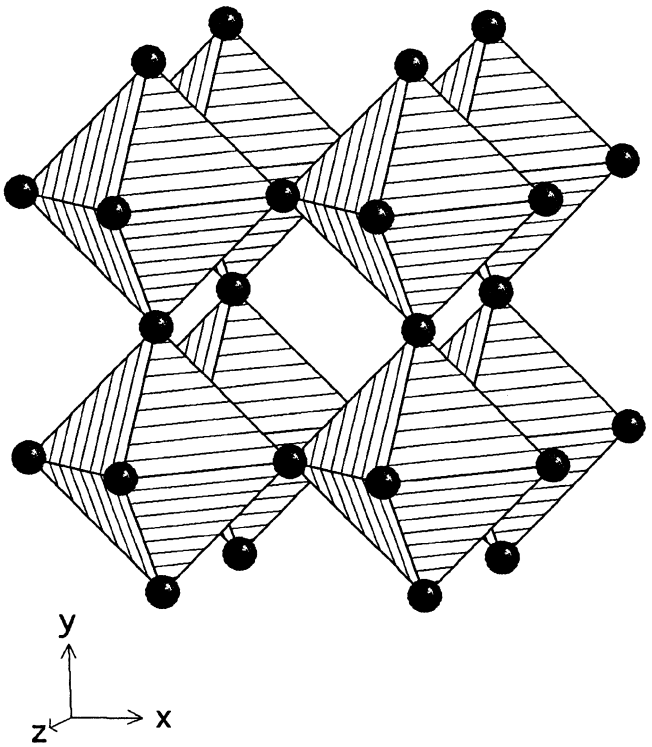

FIG. 1. Close to $\langle 001 \rangle$ projection of the $Re O_3$-type average structure of NbO_2F. The NbX_6 (X = O,F) octahedra are shown hatched.

Content Technology LLC) and Adobe photoshop were used to enhance the visibility of the weaker diffraction features for presentation in the printed form.

ELECTRON DIFFRACTION RESULTS

Careful investigation of the reciprocal lattice of NbO_2F showed a complex mixture of diffraction features in addition to the strong underlying parent reflections of the $Re O_3$-type average structure (hereafter labelled **G**) (see Figs. 2 and 3). The most prominent of these features is the existence of strong, transverse polarized lines of diffuse streaking running along all $\langle hk0 \rangle$* type directions of reciprocal space and which become particularly prominent at large **g** (see for example Figs. 2 and 3). In addition, there are often what appear to be sharp additional superlattice reflections (some examples of which are arrowed in Figs. 2 and 3) in many zone axis electron diffraction patterns (EDPs), whilst in others (Figs. 2b and 3b) diffuse dashes of short duration can also be observed. Careful consideration of many such EDPs shows that these features can only be explained in terms of the simultaneous presence of planes of diffuse intensity co-existing with rods of diffuse intensity. It is believed that these two types of diffuse distribution arise from a quite distinct crystal chemical origin (see below). We begin with the planar diffuse.

Planar Diffuse

Figure 2a shows a typical (relatively close to) $\langle 001 \rangle$ zone axis electron diffraction pattern (EDP). In addition to the average structure Bragg reflections, strong continuous transverse polarized lines of diffuse intensity are observed to

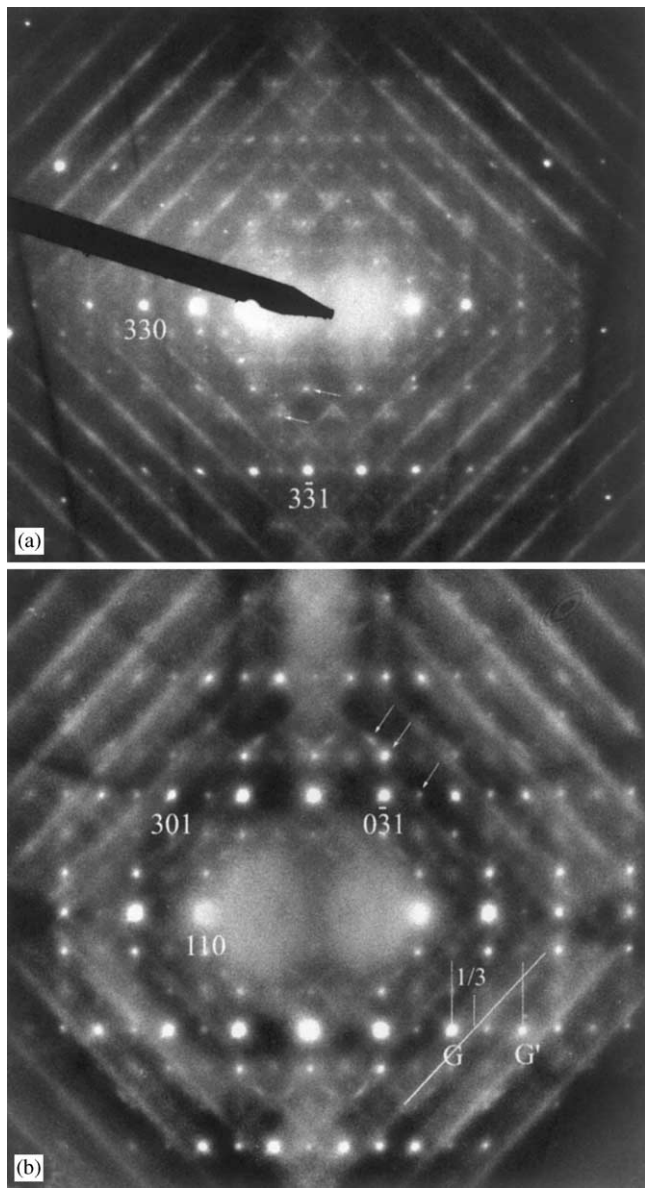

FIG. 2. Shows typical (a) close to $[\bar{1}16]$ and (b) $[\bar{1}13]$ zone axis EDPs for NbO_2F. In each case strong, essentially continuous, transverse polarized, diffuse streaking along the $[h0l]$* and $[0kl]$* directions of reciprocal space are clearly visible, particularly at large **g**. Note that this characteristic diffuse streaking does not go through the parent Bragg reflections **G** but instead can always be observed to run through positions at $\frac{1}{3}$ of the distance between neighboring parent Bragg reflections (see Fig. 2b). Note also that it only appears to occur on the high angle (i.e., the $\mathbf{G} + \frac{1}{3}(\mathbf{G} - \mathbf{G}')$) side of the parent Bragg reflections. Finally, note the many additional 'satellite reflections' as indicated by the arrows.

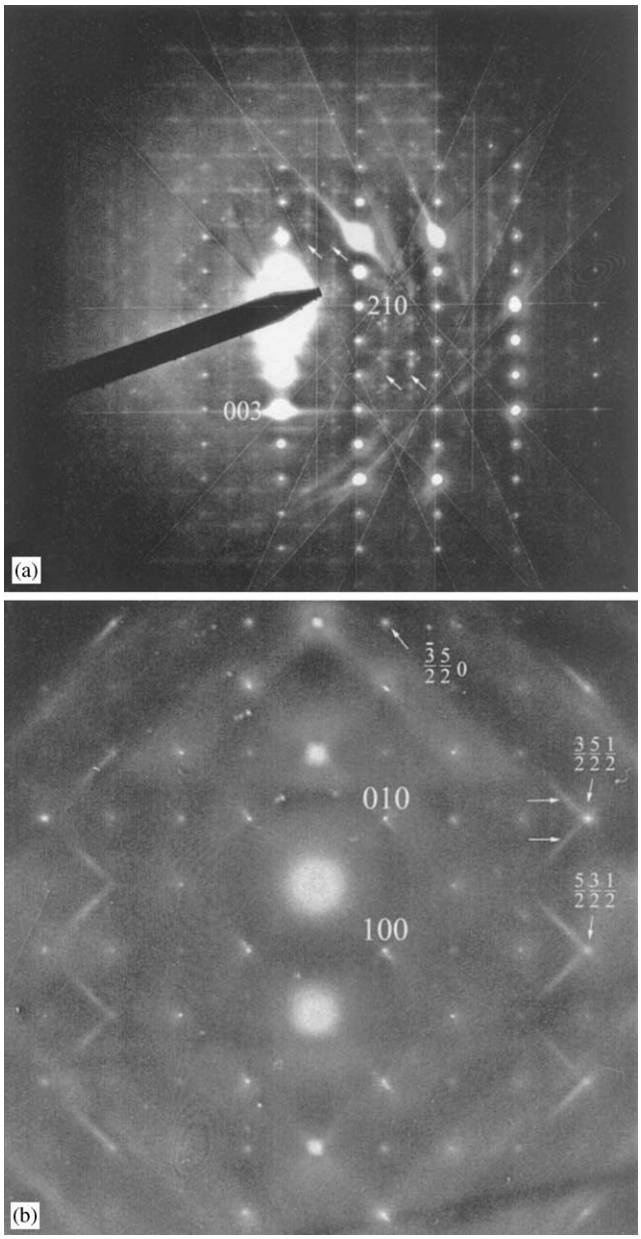

FIG. 3. Selected area EDPs taken close to (a) a $\langle 120 \rangle$ zone axis orientation and (b) a $\langle 118 \rangle$ orientation (within $\sim 10^\circ$ of an $\langle 001 \rangle$ zone axis orientation). Note that the weaker features of reciprocal space can often be made more prominent relative to the rather stronger Bragg reflections of the underlying average structure by deliberately tilting slightly off exact zone axis orientations. The Kikuchi bands in (a) have been highlighted in order to avoid confusion with the diffuse streaking running along the [210]* and [001]* directions of reciprocal space. Note the apparent 'satellite reflections' at $\frac{1}{2}$ [351]* and $\frac{1}{2}$ [$\bar{3}$50]* (arrowed in Fig. 3b) as well as the extended diffuse dashes (also arrowed in Fig. 3b) emanating from $\mathbf{G} \pm \frac{1}{2}$ [351]*.

run along both the [601]* and [0$\bar{6}$1]* directions of reciprocal space. Such [*h*0*l*]* and [0*kl*]* lines of diffuse intensity ($\langle hk0 \rangle$* in general) continue to remain no matter how far we tilt around the $\langle 110 \rangle$* systematic row. In the [$\bar{1}$13] zone axis EDP of Fig. 2b, for example, these diffuse lines, or streaks, can still be observed, but this time running along the [301]* and [03$\bar{1}$]* directions of reciprocal space. In general, the diffuse streaking is always observed to run along all $\langle hk0 \rangle$* directions of reciprocal space, which can only be interpreted in terms of the existence of planes, or sheets, of diffuse intensity running through reciprocal space which are orthogonal to each of the major **a**, **b** and **c** crystal directions.

There are several very important things to note about the diffuse streaking. The first is that it does not go through the parent Bragg reflections but instead can always be observed to run through positions at $\frac{1}{3}$ of the distance between neighboring parent Bragg reflections (see, for example, Fig. 2). First impressions suggest that this diffuse streaking only ever appears only on the high angle side (i.e., on the $\mathbf{G} + \frac{1}{3}(\mathbf{G}' - \mathbf{G})$ side) of the parent reflections (see Fig 2b). Careful examination of the close to [$\bar{1}$20] zone axis EDP of Fig. 3a, however (see the arrows), shows that the streaking can appear on both the high as well as the low angle (i.e., $\mathbf{G} - \frac{1}{3}(\mathbf{G}' - \mathbf{G})$) side of the parent Bragg reflections, particularly when viewed closer to the origin of reciprocal space. This suggests the diffuse planes, in general, exist at reciprocal space positions $\mathbf{G} \pm \langle hk\frac{1}{3} \rangle$*, where *h* and *k* here are understood to be able to take on any value. The apparent absence of the $\mathbf{G} - \langle hk\frac{1}{3} \rangle$*diffuse streaking on the low angle side of the parent reflections in Fig. 2 must therefore be due to a structure factor effect. In fact, the asymmetric nature of the intensity of the diffuse streaking as observed in the majority of the patterns is thought to be due to the so-called 'atomic size effect' (16, 17) which is a characteristic of systems exhibiting large displacive relaxations and results in a transfer of diffuse intensity from the low to the high angle side (or vice versa) of the parent reflections (more on this later).

The second very important thing to note about the diffuse streaking is that there is a very strong angular, or azimuthal, character to it indicating that atomic displacements make the largest direct contribution to the observed diffuse intensity distribution. Consider the observed diffuse distribution from a modulation wave point of view (18) whereby each point on the observed diffuse distribution is described as $\mathbf{G} \pm \mathbf{q}$ and the various $\mathbf{q} = \langle hk\frac{1}{3} \rangle$* modulations are treated as independent modulation waves. Following (18), the displacive contribution to the kinematic structure factor at $(\mathbf{G} + \mathbf{q})$ is given by

$$F_{\text{disp}}(\mathbf{G} + \mathbf{q}) \propto \textstyle\sum_\mu f_\mu^{\text{av}} \exp\{2\pi \text{i} \mathbf{G} \cdot \mathbf{r}_\mu\} 2\pi(\mathbf{G} + \mathbf{q}) \cdot \mathbf{e}_\mu(\mathbf{q}) + \cdots,$$

where $\mathbf{r}_\mu$ labels the position of the μth atom in the parent unit cell and $\mathbf{e}_\mu(\mathbf{q})$ represents the displacement eigenvector (or shift of this atom) associated with the modulation wave vector $\mathbf{q}$. It is the dot product $(\mathbf{G} + \mathbf{q}) \cdot \mathbf{e}_\mu(\mathbf{q})$ in the above

kinematic structure factor expression that gives rise to the observed strong azimuthal intensity variation in Fig. 2. The transverse polarized nature of this streaking (i.e., the fact that the intensity of the diffuse streaking is always strongest at reciprocal space positions ($\mathbf{G} + \mathbf{q}$) perpendicular to the direction of the streaking itself and zero at reciprocal space positions ($\mathbf{G} + \mathbf{q}$) parallel to the direction of the streaking) requires that the associated atomic shifts must also be transverse polarized, i.e., the atomic shifts giving rise to the $\mathbf{G} \pm \langle hk\frac{1}{3}\rangle^*$ diffuse planes perpendicular to $\langle 001\rangle$ must be due to atomic shifts along $\langle 001\rangle$ (i.e., along **a**, **b** and **c**).

Rods of Diffuse

The remaining (initially unexpected) diffraction features visible in Figs. 2 and 3 (e.g., the arrowed $\mathbf{G} \pm \frac{1}{2}[3\bar{3}1]^*$ and $\mathbf{G} \pm \frac{1}{2}[9\bar{3}2]^*$ 'satellite reflections' of Fig. 2a or the also arrowed $\mathbf{G} \pm \frac{1}{6}$ $[3\bar{3}2]^*$ and $\mathbf{G} \pm \frac{1}{2}$ $[110]^*$ 'satellite reflections' and the short diffuse dashes of Fig. 2b) can all be described in terms of essentially continuous diffuse streaking along the three $\langle 001\rangle^*$ directions of reciprocal space associated with modulation wave vectors this time of type $\langle\frac{1}{2}, \frac{1}{2}, \xi\rangle^*$ (ξ is here understood to be a continuous variable) and running through the $\mathbf{G} \pm \langle\frac{1}{2}, \frac{1}{2}, \xi\rangle^*$ regions of reciprocal space. Note that the three diffuse rods intersect at $\mathbf{G} \pm \frac{1}{2}$ $[111]^*$ positions of reciprocal space.

An excellent example can be seen in the case of the $\mathbf{G} \pm \frac{1}{2}$ $[351]^*$ and $\mathbf{G} \pm \frac{1}{2}$ $[\bar{3}50]^*$ type 'satellite reflections' of Fig. 3b. In the case of the latter 'satellite reflection', the associated diffuse rod runs along the $[001]^*$ direction of reciprocal space. Because the diffracting plane in Fig. 3b cuts across these $\mathbf{G} \pm [\frac{1}{2}, \frac{1}{2}, \xi]^*$ diffuse rods at a rather large angle ($\sim 80^\circ$), they give rise to what appear to be sharp 'satellite reflections'. In the case of the $\mathbf{G} \pm \frac{1}{2}$ $[351]^* \equiv \mathbf{G}' \pm \frac{1}{2}$ $[111]^*$ 'satellite reflection', all three diffuse rods intersect at this point. The $[\frac{1}{2}, \frac{1}{2}, \xi]^*$ diffuse rod runs along $[001]^*$ and hence gives rise to what appears to be a sharp 'satellite reflection'. By contrast, the diffuse dashes (also arrowed in Fig. 3b) emanating from $\mathbf{G} \pm \frac{1}{2}$ $[351]^*$ are associated with the two remaining $[\xi, \frac{1}{2}, \frac{1}{2},]^*$ and $[\frac{1}{2}, \xi, \frac{1}{2},]^*$ diffuse rods running along the $[100]^*$ and $[010]^*$ directions of reciprocal space. Because the diffracting plane in Fig. 2b cuts across these $\mathbf{G} \pm [\xi, \frac{1}{2}, \frac{1}{2},]^*$ and $\mathbf{G} \pm [\frac{1}{2}, \xi, \frac{1}{2},]^*$ diffuse rods at a rather more acute angle ($\sim 7^\circ$), they give rise to considerably extended diffuse dashes.

Finally, note that the atomic shifts associated with these $\langle\frac{1}{2}\frac{1}{2}\xi\rangle^*$ diffuse rods must be transverse polarized, i.e., orthogonal to the streak direction. That this is the case is experimentally clear from Figs. 2 and 3. If we look out from the origin of reciprocal space along the $[010]^*$ direction of reciprocal space in Fig. 3b, for example, then the strongest diffuse streaking is observed along the orthogonal $[100]^*$ direction of reciprocal space and vice versa.

INTERPRETATION

Having established that the reciprocal lattice of NbO_2F is characterized by both planes as well as rods of diffuse intensity, the question now becomes what is the crystal chemical origin of these observed diffraction effects. Again, we begin with the explanation of the planar diffuse.

Planar Diffuse

It is well known that the occurrence of planes of diffuse intensity at $\mathbf{G} \pm \langle hk\frac{1}{3}\rangle^*$ positions of reciprocal space implies the existence of one-dimensional columns of atoms along $\langle 001\rangle$ whose occupancies and atomic positions are correlated along each column but without any lateral correlation from one such column to the next. The $\frac{1}{3}$ **c*** component of these sheets, in turn, implies that the occupancies and displacements of the atoms along each $\langle 001\rangle$ column give rise to a 3 times supercell along this direction. In addition, the observed transverse polarized nature of the diffuse streaking implies that atomic shifts along the column direction, i.e., along $\langle 001\rangle$, make the major contribution to the observed diffuse.

A further clue can be found in the asymmetric nature of the intensity distribution of the diffuse streaking on either side of the parent reflections (see Fig. 2). As mentioned previously, these are reminiscent of the so-called 'atomic size effect' (16, 17). The atomic size effect is normally attributed to a correlation or coupling between compositional and displacive modulations associated with the same modulation wave vector and which give rise to the well known and characteristic effect of transferring intensity from regions on one side of the parent Bragg reflection to regions on the other (16, 17).

In the case of NbO_2F, we could think of this in terms of oxygen–fluorine ordering giving rise to displacive relaxation of the Nb cations. However, in this case any cross terms involving oxygen/fluorine compositional ordering (16, 17) are unlikely to contribute significantly to a 'size effect' intensity redistribution due to the similarity in electron scattering factor for both these anions. This leaves higher-order terms involving the displacive relaxation of the Nb atoms arising from O/F ordering as the likely predominating cause for the size effect intensity redistribution (16, 17) and also suggests that the magnitude of such displacements must be relatively large ($> \sim 3\%$ of the parent unit-cell dimension, i.e., $> \sim 0.12$ Å according to (17)). Although such displacive shifts of the Nb atoms could technically arise without an underlying compositional cause, it seems highly likely that any such Nb shifts are in direct response to oxygen/fluorine ordering in strings along the $\langle 001\rangle$ directions.

The question now becomes what can possibly give rise to a 3 times repeat along each of the $\langle 001\rangle$ real space directions? The obvious answer is oxygen/fluorine ordering and

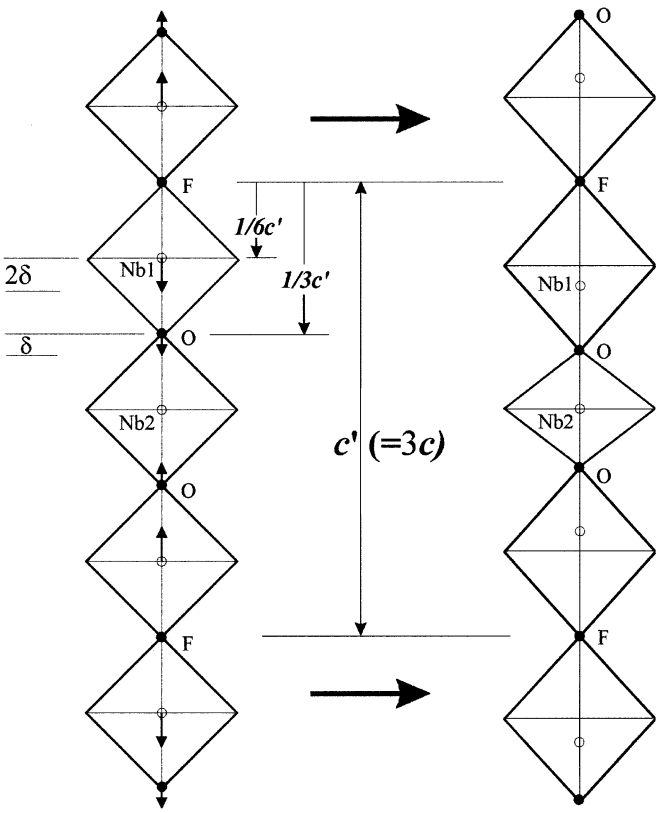

FIG. 4. Diagram showing the proposed one-dimensional pattern of O/F ordering and associated displacive relaxation of the Nb, O and F ions along $\langle 001 \rangle$ giving rise to the $\langle hk\frac{1}{3} \rangle$* sheets of diffuse intensity.

associated displacive relaxation along $\langle 001 \rangle$ (see Fig. 4) particularly given the 2:1 oxygen/fluorine ratio inherent to NbO_2F. If we apply this 2:1 ratio to produce the most obvious ordered arrangement of anions in strings along ***c***, the 3 times repeat shown in Fig. 4 results.

Using this model, the crystal chemical reasons for the proposed Nb shifts can be understood via a bond-valence analysis of the average structure of NbO_2F. Such apparent valence (AV) calculations indicate that oxygen, with a calculated AV of 1.795, is moderately underbonded in the average structure anion position while fluorine (AV = 1.607) is massively overbonded (see Table 1a). Using the R_0 parameters of Brese and O'Keeffe (9), the ideal anion to Nb^{5+} separation distance when the anion is O^{2-} should be 1.911 Å while the ideal anion to Nb^{5+} separation distance when the anion is F^- should be 2.126 Å. The anion–cation separation distance as determined from the simple ReO_3-type average structure is simply half the unit-cell dimension, or 1.951 Å.

Chemically this implies that F^- ions will strongly repel the neighboring Nb^{5+} cations while O^{2-} ions will attract them. If we consider this in relation to the proposed ordered string of ions along **c** as shown in Fig. 4, the niobium atom nearest the fluorine would need to shift out of the center of its anion octahedra towards the nearest oxygen. This oxygen, in response, will then shift towards the next niobium atom, in order to meet its optimum valence requirements. Simple geometry considerations dictate that the oxygen shift (δ) should be half the shift of the niobium atoms (2δ) as indicated in Fig. 4.

Adjusting δ such that the percentage deviation in calculated from ideal AV for each ion is the same (see Table 1b) suggests that the shift of the niobium atom towards the oxygen (2δ) would need to be -0.14 Å. (As far as the observed size effect intensity redistribution is concerned, the predicted magnitude of this shift is in good agreement with Butler and Welberry (17) who suggested the need for a $> \sim 3\%$ shift (relative to the unit-cell dimension) to account for the asymmetric diffuse scattering observed in systems exhibiting large static atomic displacements, in cases where atomic species (in this case O and F) have similar scattering factors. Intriguingly for such a value of δ, each ion is then systematically overbonded by $\sim 9\%$ (see Table 1b). (Note that such a systematic overbonding could be eliminated by an $\sim 1.6\%$ expansion of the average structure Nb–O,F bond length—see below.)

A simple one-dimensional kinematic calculation based on Fig. 4 can be used to confirm that such a magnitude of δ is entirely compatible with experimental observation. From Fig. 4, the position of the Nb, O and F ions per $\mathbf{c}' = 3\mathbf{c}_p$ supercell are as follows: F at $0\mathbf{c}'$, O's at $\pm(\frac{1}{3} + \delta)\mathbf{c}'$, Nb1's at $\pm(\frac{1}{6} + 2\delta)\mathbf{c}'$ and Nb2 at $\frac{1}{2}\mathbf{c}'$. The corresponding structure factor $F(l\mathbf{c}'^*)$ (where $\mathbf{c}'^* \equiv \frac{1}{3}\mathbf{c}_p^*$, p for parent) representing the kinematic structure factor of the $\mathbf{G} \pm \langle hk\frac{1}{3} \rangle^*$ diffuse streaking is then given by

$$F(l\mathbf{c}'^*) = f_F + 2f_O \cos 2\pi l(\tfrac{1}{3} + \delta) + f_{Nb} \cos \pi l + 2f_{Nb} \cos 2\pi l(\tfrac{1}{6} + 2\delta).$$

Table 2 lists the calculated values of this function as well as the calculated intensity asymmetries ($|F([3J + 1]\mathbf{c}'^*)|^2/$

TABLE 1
Bond Valence Sums for NbO_2F ($v = \exp[R_0 - d)/b]$, with b = 0.37 Å)

	At Nb (4O,2F)	At O	At F
(a) From average structure refinement Nb–O,F = 1.951 Å	5.197	1.795	1.607
(b) Including displacement along *c*, $\delta = 0.072$ Å Nb–O = 1.879 Å, Nb–F = 2.095 Å	5.449	2.179	1.090
(c) Including displacement along *c* and $\sim 10°$ RUM Nb–O = 1.908 Å, Nb–F = 2.127 Å	5.029	2.015	0.999
Ideal valence sum	5.000	2.000	1.000

TABLE 2
Structure Factor Calculations for NbO_2F

l	$F(lc^*)$	$I(3j+1)/I(3j-1)$
2	− 2.12	
$\mathbf{c}_p^*$	—	1.95
4	2.96	
5	3.37	
$2\mathbf{c}_p^*$	—	1.56
7	− 4.22	
8	− 1.95	
$3\mathbf{c}_p^*$	—	2.63
10	3.17	
11	2.55	
$4\mathbf{c}_p^*$	—	1.88
13	− 3.49	
14	− 0.96	
$5\mathbf{c}_p^*$	—	7.24
16	2.58 −	
17	1.47	
$6\mathbf{c}_p^*$	—	3.30
19	− 2.67	
20	− 0.26	
$7\mathbf{c}_p^*$	—	61.03
22	2.01	
23	0.64	
$8\mathbf{c}_p^*$	—	9.66
25	− 1.98	
26	0.24	
$9\mathbf{c}_p^*$	—	36.12
28	1.45	
29	0.084	
$10\mathbf{c}_p^*$	—	256.38
31	− 1.35	

($|F([3J-1]\mathbf{c}'^*)|^2$, i.e., either side of the parent reflections) for values of $l = 3J \pm 1$ (and $\delta = 0.072$ Å) using electron scattering factors taken from the International Tables for Crystallography (19). It can readily be seen that intensity is predicted to be systematically transferred from the low to the high angle side of the parent Bragg reflections, most markedly at large **g**, just as is observed experimentally (cf. Fig. 2). While it is acknowledged that dynamical scattering probably does perturb the observed intensity asymmetries away from the kinematic values of Table 2, it is nonetheless clear that the predicted magnitude of δ is in good qualitative agreement with experimental observation. Reversing the sign of δ, for example, would completely reverse the intensity asymmetry from what is observed experimentally.

Rods of Diffuse

The existence of transverse polarized lines of diffuse intensity running along the $\mathbf{G} \pm \langle \frac{1}{2}, \frac{1}{2}, \xi \rangle^*$ directions of reciprocal space can, we believe, be associated with presence of the so-called Rigid Unit Mode or RUM (6, 20, 21) modes. Whenever octahedra are corner-connected as in the ReO_3 structure type there is inherent rotational flexibility, which requires very little energy to be thermally excited and does not distort the constituent octahedra, at least for a small amplitude of rotation (see Fig 5). In the case of perovskites, the existence of such low-frequency rotational modes have been well documented both theoretically and experimentally (6, 20, 22). Octahedral rotation around **c**, for example, necessarily gives rise to a correlated $2\times$ repeat along the orthogonal [100] and [010] directions (see Fig. 5). Because the axis of rotation is perpendicular to the (001) plane, however, there is no necessary correlated coupling of this rotation along the [001] direction itself (see Fig. 5b), i.e., there is a correlated displacement (of the anions) within the (001) type planes but no correlation from one such plane to the next. In reciprocal space, this manifests itself in the presence of rods of diffuse intensity (19, 20) parallel to **a***, **b*** and **c*** associated with modulation wave vectors of $\langle \frac{1}{2}, \frac{1}{2}, \xi \rangle^*$ type. Note that the atomic shifts associated with these $\langle \frac{1}{2}, \frac{1}{2}, \xi \rangle^*$ RUM modes are transverse polarized, i.e., orthogonal to the streak direction (see Fig. 5a) just as is required experimentally—see above. The condensation of just such a $[\frac{1}{2}, \frac{1}{2}, \frac{1}{2}]^*$ RUM mode is responsible for the recently observed pressure-induced phase transformation of NbO_2F (5).

For infinitesimally small amplitudes of rotation, the local Nb–anion distances will be unaffected. If the local amplitude of octahedral rotation is sufficiently large, however, then the local Nb–anion distances will be larger than one-half of the refined average structure unit-cell dimension, i.e., the 'effective' average structure unit-cell dimension (to be used for bond-valence calculations) should be increased (see Fig. 6). It is worth noting that a 1.6% increase in the effective unit-cell dimension (from 3.902 to 3.966 Å), corresponding to an average RUM rotation angle of $\sim 10^\circ$ and arising from the presence of RUM modes (whether static or dynamically excited), would be sufficient for each of the $\sim 9\%$ overbonded AVs in Table 1b to be reduced to their nominally ideal values (see Table 1c).

The question of whether these RUM modes are necessarily dynamically excited or might instead be statically condensed in some sort of twinned micro-domain model is strongly reminiscent of a similar argument that has raged for many years as to the exact nature of the high-temperature polymorphic forms of the cristobalite and tridymite tetrahedral framework structures. In those cases, recent experimental and theoretical work has, we believe, demonstrated conclusively that the dynamically excited RUM approach is the correct one (see, for example, the discussions given in Refs. 23 and 24 and other references contained therein). In the case of NbO_2F, the relevant experimental and theoretical work has yet to be carried out and so we cannot *a priori* rule out a static microdomain-type model at

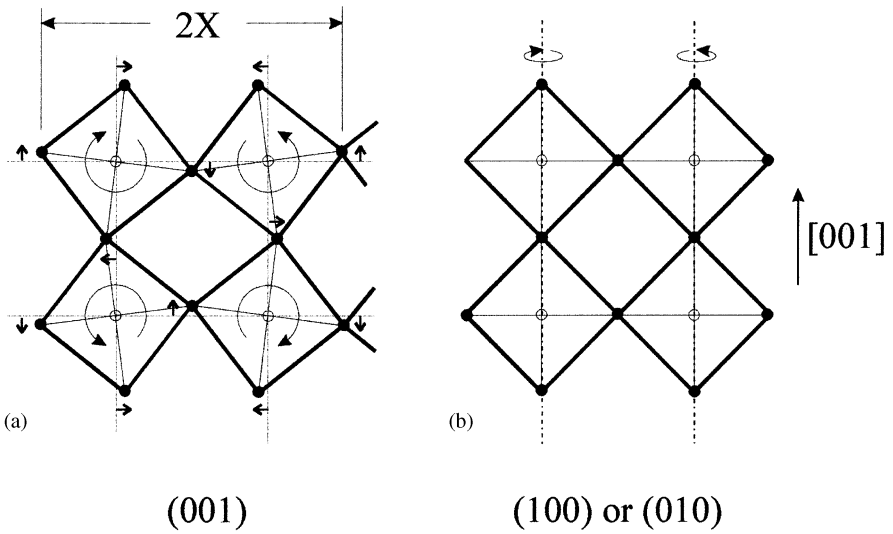

FIG. 5. Diagrams showing how a correlated RUM rotation of NbX_6 octahedra about the c axis (a) results in a repeated (2X) pattern of displacements along the orthogonal [100] and [010] directions. The same rotation does not, however, necessitate correlated shifts along [001] (see (b)). Dynamic excitation of such RUM modes of distortion gives rise to diffuse rods running along the $\mathbf{G} \pm \langle \frac{1}{2}\frac{1}{2}\zeta \rangle^*$ regions of reciprocal space. Note that the atomic shifts associated with $\langle \frac{1}{2}\frac{1}{2}\zeta \rangle^*$ RUM's are transverse polarized, i.e., orthogonal to the streak direction.

this stage. Nonetheless, the more or less uniform intensity distribution along the $\mathbf{G} \pm \langle \frac{1}{2}, \frac{1}{2}, \zeta \rangle^*$ diffuse streaks of Fig. 3b coupled with the reversibility of the recently observed pressure-induced phase transformation of NbO_2F (arising from the freezing-in or condensation of a specific $[\frac{1}{2}, \frac{1}{2}, \frac{1}{2}]^*$ RUM mode at the pressure-induced phase transition) strongly suggests to us that the ambient pressure, room temperature phase is dynamically rather than statically disordered.

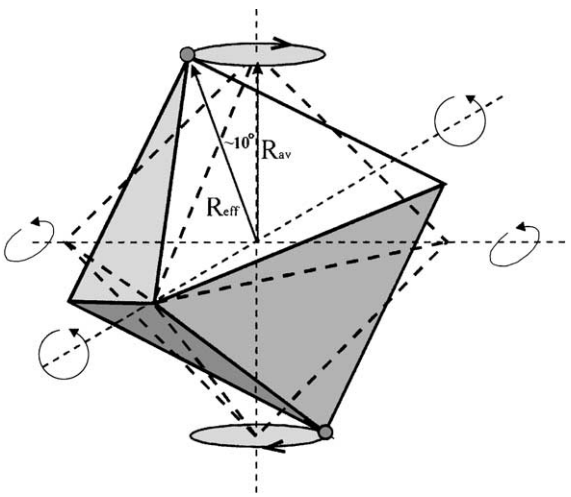

FIG. 6. Diagram showing the rotation of the anion around the refined average position due to octahedral rotations (RUMs). It is the effective Nb–O,F distance (R_{eff}) which should be considered in the bond-valence calculations.

What is being proposed is that each anion is on average precessing on an annulus around the refined average anion position with an annulus radius corresponding to $\sim 10^\circ$ as a result of the dynamic excitation of RUM modes such that the local Nb-X-Nb angle is more like 160 than 180°. This is very similar to what has been proposed for disordered silicas such as cristobalite and tridymite in their high-symmetry polymorphic forms (23, 24).

CONCLUSIONS

Our final conclusion is that there is clear diffraction evidence, in the form of observed $\langle hk\frac{1}{3} \rangle^*$ sheets of diffuse intensity, that O and F are indeed ordered in NbO_2F, but only in one-dimensional strings along each of the three $\langle 001 \rangle$ directions. Under the zeroth order assumption that there is absolutely no correlation in this O/F ordering not only from one string to the next along the same $\langle 001 \rangle$ direction but between strings along different $\langle 001 \rangle$ directions, the most probable local octahedral stoichiometry around an Nb ion is then O_4F_2 at $P(NbO_4F_2) = \frac{12}{27}$. The only other possibilities are as follows: $P(NbO_3F_3) = \frac{8}{27}$, $P(NbO_5F) = \frac{6}{27}$ and $P(NbO_6) = \frac{1}{27}$. Provided that the atoms locally relax as shown in Fig. 4 along all three $\langle 001 \rangle$ directions simultaneously there would also seem to be no real driving force or need for three-dimensional long-range order in the conventional crystallographic sense.

The co-existence of transverse polarized $\langle \frac{1}{2}, \frac{1}{2}, \zeta \rangle^*$ type diffuse scattering implies the simultaneous co-existence of

(presumably dynamically excited) RUM-type modes whose influence seems to locally expand the size of the NbX_6 polyhedra to the ideal size from the bond-valence point of view (see Table 1c). As in our previous work on FeOF (13), it would seem that it is very important to take structured diffuse intensity distributions into account in oxyfluoride systems if the local O/F ordering pattern is to be understood.

REFERENCES

1. L. K. Frevel and H. W. Rinn, *Acta Crystallogr.* **9,** 626–627 (1956).
2. A. W. Sleight, *Inorg. Chem.* **8**(8), 1764–1767 (1969).
3. L. Permér and M. Lundberg, *J. Solid State Chem.* **81,** 21–29 (1989).
4. C. Bohnke, J. L. Fourquet, N. Randrianantoandro, T. Brousse, and O. Crosnier, *J. Solid State Electrochem.* **5,** 1–7, 2001.
5. S. Carlson, A.-K. Larsson, and F. E. Rohrer, *Acta Crystallogr. B* **56,** 189–196 (2000).
6. M. Dove, *Am. Miner.* **82,** 213–244 (1997).
7. P. Hagenmuller, *in* "Perspectives in solid state chemistry" (K. J. Rao, Ed.), pp. 66–78. Narosa, New Delhi, 1995.
8. T. Vogt, P. M. Woodward, B. A. Hunter, A. K. Prodjosantoso, and B. J. Kennedy, *J. Solid State Chem.* **144,** 228–231 (1999).
9. N. E. Brese and M. O'Keeffe, *Acta Crystallogr. B* **47,** 192 (1991).
10. D. Suter and R. Ernst, *Phys. Rev. B* **32,** 5608 (1985).
11. L. Du, F. Wang, and C. P. Grey, *J. Solid State Chem.* **140,** 285–294 (1998).
12. R. L. Needs and M. T. Weller, *J. Chem. Soc. Dalton Trans.* 3015–3017 (1995).
13. F. J. Brink, R. L. Withers, and J. G. Thompson, *J. Solid State Chem.* **155,** 359–365 (2000).
14. L. Du, A. Samoson, T. Tuherm, and C. P. Grey, *Chem. Mater.* **12,** 3611–3616 (2000).
15. J. Chappert and J. Portier, *Solid State Commun.* **4,** 185 (1966).
16. B. D. Butler and T. R. Welberry, *Acta Crystallogr. A* **49,** 736–743 (1993).
17. B. D. Butler, R. L. Withers, and T. R. Welberry, *Acta Crystallogr. A* **48,** 737 (1992).
18. R. L. Withers, S. Schmid, and J. G. Thompson, *Prog. Solid State Chem.* **26,** 1–96 (1998).
19. T. Hahn (Ed.), "International Tables for Crystallography," Vol. A. Kluwer Academic, Dordrecht, 1992.
20. K. D. Hammonds, M. T. Dove, A. P. Giddy, V. Heine, and B. Winkler, *Am. Mineral.* **81,** 1057–1079 (1996).
21. A. P. Giddy, M. T. Dove, S. Pawley, and V. Heine, *Acta Crystallogr. A* **49,** 697–703 (1993).
22. A. M. Glazer, *Acta Crystallogr. B* **28,** 3384–3392 (1972).
23. J. G. Thompson, R. L. Withers, S. R. Palethorpe, and A. Melnitchenko, *J. Solid State Chem.* **141,** 29–49 (1998).
24. M. Dove, A. K. A. Pryde, and D. A. Keen, *Miner. Maga.* **64,** 267–283 (2000).